Inorganic Chemistry

Article

pubs.acs.org/IC

# Tetranuclear Iron Complexes Bearing Benzenetetrathiolate Bridges as Four-Electron Transformation Templates and Their Electrocatalytic Properties for Proton Reduction

Lin Chen,[†] Mei Wang,*[,†] Frederic Gloaguen,[‡] Dehua Zheng,[†] Peili Zhang,[†] and Licheng Sun*[,†,§]

[†]State Key Laboratory of Fine Chemicals, DUT-KTH Joint Education and Research Center on Molecular Devices, Dalian University of Technology, Dalian 116024, People's Republic of China

[‡]UMR 6521, CNRS, Université de Bretagne Occidentale, CS 93387, 29238 Brest, France

[§]Department of Chemistry, KTH Royal Institute of Technology, 10044 Stockholm, Sweden

Supporting Information

**ABSTRACT:** Two tetranuclear iron–sulfur complexes, ($\mu,\mu$-pbtt)[$Fe_2(CO)_6$]$_2$ (pbtt = benzene-1,2,4,5-tetrathiolato, **3**) and ($\mu,\mu$-obtt)[$Fe_2(CO)_6$]$_2$ (obtt = benzene-1,2,3,4-tetrathiolato, **4**), were prepared from reaction of $Fe_3(CO)_{12}$ and the corresponding tetramercaptobenzene in THF, respectively. Complexes **5** and **6**, ($\mu,\mu$-pbtt)[$Fe_2(CO)_5L^1$][$Fe_2(CO)_5L^2$] ($L^1$ = CO, $L^2$ = $PPyr_3$ (Pyr = *N*-pyrrolyl), **5**; $L^1 = L^2 = PPyr_3$, **6**) were obtained by controlling CO displacement of **3** with $PPyr_3$. Molecular structures of **3**–**6** were determined by spectroscopic and single-crystal X-ray analyses. All-CO $Fe_4S_4$ complexes **3** and **4** each display four-electron reduction processes in consecutive chemically reversible two-electron reduction events with relatively narrow potential spans in the cyclic voltammograms. Phosphine-substituted $Fe_4S_4$ complexes **5** and **6** exhibit two consecutive two-electron reduction events, which are not fully reversible. The electrocatalytic properties of **3** and **4** for proton reduction were studied using a series of carboxylic acids of increasing strength ($CH_3COOH$, $CH_2ClCOOH$, $CHCl_2COOH$, $CCl_3COOH$, and $CF_3COOH$). The mechanisms for electrochemical proton reduction to hydrogen catalyzed by complex **3** as a function of acid strength are discussed.

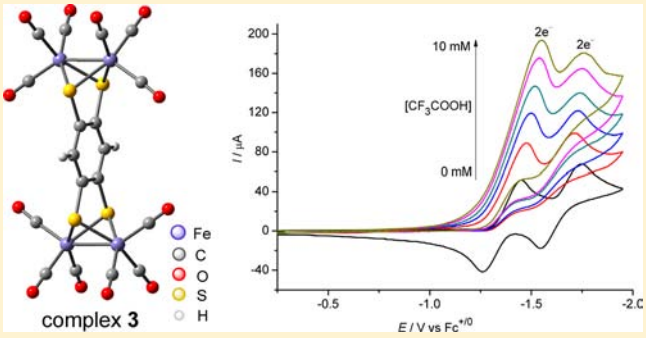


## INTRODUCTION

Polynuclear iron–sulfur cofactors in the active sites of metalloproteins often play a key role in biological redox reactions,[1−3] for example, in the reduction of protons to dihydrogen by the FeFe-hydrogenase and carbon dioxide to carbohydrates in photosystem I.[4,5] In view of functional mimics of multielectron redox properties of metalloenzymes, polynuclear iron–sulfur complexes that may act as templates for multielectron transformations are of great interest. In the past decade, synthesis and chemistry of FeFe- and NiFe-hydrogenase active site mimics have attracted special attention as they are related to $H_2$ production and activation. Studies on the properties and chemistry of bioinspired FeFe and NiFe complexes aim at developing iron-based electro- and photochemical catalyst systems for $H_2$ production and at better understanding the mechanism of enzymatic $H_2$ formation and uptake.

In recent years, a large number of structural and functional models of the FeFe-hydrogenase active site were reported and their electrochemistry was extensively studied.[6−11] Most reported iron–sulfur mimics act as two-electron relays by two one-electron transformations.[12−17] It was found that introduction of a rigid and conjugate bridge to the $Fe_2S_2$ complexes could make the electrochemical properties of the complexes apparently different from the $Fe_2S_2$ complexes with flexible bridges,[18−21] either $SCH_2CH_2CH_2S$ or $SCH_2NRCH_2S$ bridge. For example, the well-known complex ($\mu$-pdt)[$Fe_2(CO)_6$] (pdt = propane-1,3-dithiolato) displays an initial one-electron reduction event at −1.74 V (all potentials mentioned in this paper are versus $Fc^+$/Fc) and a second irreversible reduction event at the potential 0.6 V more negative than the initial reduction event,[13,22] while the complex ($\mu$-bdt)[$Fe_2(CO)_6$] (**1**, Figure 1) with a benzene-1,2-dithiolate (bdt) bridge is reduced to its dianion in a chemically reversible two-electron process at −1.44 V in $CH_2Cl_2$.[18] The reduced species of **1** is strongly stabilized by the rigid and conjugate benzene bridge. The special electrochemical property makes complex **1** a robust proton reduction catalyst operating at a mild potential for electrochemical hydrogen production in organic solvent[18−21] and aqueous micellar solution.[23] Such type of $Fe_2S_2$ complexes are also promising catalysts for photochemical hydrogen production. Recently, Hammarström and Ott reported that the diiron 3,6-dichlorobenzene-1,2-dithiolate ($Cl_2$bdt) complex ($\mu$-$Cl_2$bdt)[$Fe_2(CO)_6$] (**2**, Figure 1) displayed much higher activity for photoinduced hydrogen

**Received:** July 26, 2012
**Published:** January 31, 2013

   dx.doi.org/10.1021/ic301647u | *Inorg. Chem.* 2013, 52, 1798−1806

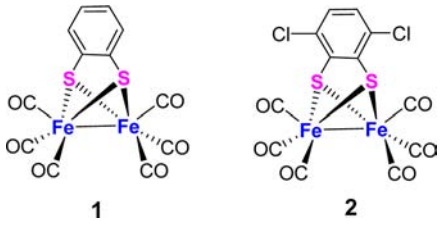


**Figure 1.** Structures of complexes **1** and **2** containing bdt and $Cl_2$bdt bridges.

production, with $[Ru(bpy)_3]^{2+}$ as photosensitizer and ascorbate as sacrificial electron donor in DMF/$H_2O$,[24] as compared to other bio-inspired all-carbonyl $Fe_2S_2$ complexes with flexible dithiolate bridges.

In these contexts, we were interested in the preparation of polynuclear iron−sulfur complexes with a rigid and conjugate bridge. Here we describe the preparation and structures of tetranuclear iron complexes ($\mu$,$\mu$-pbtt)$[Fe_2(CO)_6]_2$ (pbtt = benzene-1,2,4,5-tetrathiolato, **3**), ($\mu$,$\mu$-obtt)$[Fe_2(CO)_6]_2$ (obtt = benzene-1,2,3,4-tetrathiolato, **4**), and ($\mu$,$\mu$-pbtt)-$[Fe_2(CO)_5L^1][Fe_2(CO)_5L^2]$ ($L^1$ = CO, $L^2$ = $PPyr_3$, Pyr = *N*-pyrrolyl, **5**; $L^1$ = $L^2$ = $PPyr_3$, **6**, Figure 2). The electrochemical

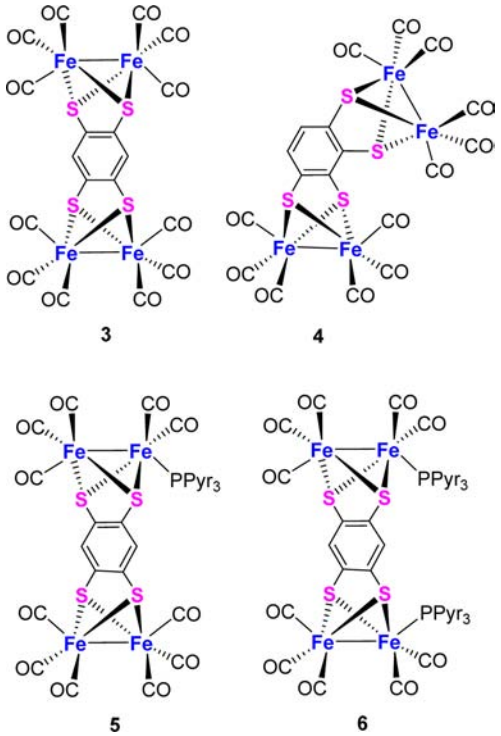


**Figure 2.** Structures of tetranuclear $Fe_4S_4$ complexes **3**−**6**.

properties of **3**−**6** and the electrocatalytic behaviors of **3** and **4** for proton reduction were studied using a series of carboxylic acids of increasing strength ($CH_3COOH$, $CH_2ClCOOH$, $CHCl_2COOH$, $CCl_3COOH$, and $CF_3COOH$). These iron complexes display two chemically reversible two-electron reduction events with relatively narrow potential spans. Complexes **3** and **4** display comparatively higher activity with mild overpotential for electrochemical proton reduction in the presence of $CF_3COOH$ in $CH_2Cl_2$.

## RESULTS AND DISCUSSION

**Preparation and Spectroscopic Characterization of Complexes 3−6.** The tetranuclear iron complex **3** was prepared in a moderate yield (62%) by treatment of $Fe_3(CO)_{12}$ with 1,2,4,5-tetramercaptobenzene in THF (Figure 2). After the reaction was carried out in refluxing THF for 24 h, each side of the benzene ring with two ortho mercapto groups is coordinated to a $Fe_2(CO)_6$ unit. Complex **4** was prepared in a yield of 32% in the similar procedure using 1,2,3,4-tetramercaptobenzene in toluene at reflux for 2 h. Tris(*N*-pyrrolyl)phosphine-mono- and disubstituted complexes, **5** and **6**, were readily prepared via CO displacement of **3** in toluene by controlling the loading amount of the $PPyr_3$ ligand. The monosubstituted complex **5** was obtained in a moderate yield (63%), while the disubstituted complex **6** was attained in a low yield (41%). TLC analysis showed that there still existed small amounts of unreacted complex **3** and monosubstituted complex **5** after the toluene solution of **3** and 2 equiv of $PPyr_3$ was refluxed for 72 h. These benzene-bridged $Fe_4S_4$ complexes are air stable both in solution and in the solid state.

Complexes **3**−**6** were characterized by IR, HR-MS, $^1H$ and $^{31}P\{^1H\}$ NMR spectroscopy, as well as elemental analysis. The $[M]^+$ peak found at $m/z$ = 761.5863 for **3** and the $[M - CO]^+$ peak at $m/z$ = 733.5926 for **4** are consistent with the calculated values. The results of the elemental analyses for complexes **5** and **6** are in good agreement with the supposed compositions. The all-carbonyl tetranuclear iron complexes **3** and **4** display four and three CO absorptions, respectively, in the region of 1980−2080 $cm^{-1}$.[25] Displacement of a CO in **3** by a $PPyr_3$ ligand disturbs the symmetric structure of the integral molecule. Accordingly, $PPyr_3$-monosubstituted complex **5** displays six CO bands in the region of 1960−2080 $cm^{-1}$, and $PPyr_3$-disubstituted tetrairon complex **6** displays four CO absorptions at 2057, 2008, 1983, and 1963 $cm^{-1}$, indicating that two monosubsituted $Fe_2(CO)_5PPyr_3$ units are connected to the benzene-1,2,4,5-tetrathiolate bridge in **6** to form a symmetric structure. Compared with the red shifts (28−32 $cm^{-1}$) of the first CO bands resulting from CO displacement of the all-carbonyl diiron dithiolate complex by $PPh_3$ and $P(OEt)_3$,[26,27] the red shift (21 $cm^{-1}$) of the first CO band caused by $PPyr_3$ is relatively small for complex **6**. The shift values of CO bands indicate that $PPyr_3$ is a weaker electron donor than $PPh_3$ and $P(OEt)_3$. In addition, only one $^{31}P$ NMR signal is observed in the $^{31}P\{^1H\}$ NMR spectrum of **6**, suggesting that the two $PPyr_3$ ligands in complex **6** have the same chemical environment. The positions of the two $PPyr_3$ ligands in complex **6** were further determined by single-crystal X-ray diffraction.

**Molecular Structures of 3−6.** The molecular structures of **3**−**6** are presented in Figure 3, and selected bond lengths and angles are listed in Table 1. The molecules of complexes **3**−**6** each have two $Fe_2S_2$ cores, which are in the similar butterfly conformation as previously reported for the diiron dithiolate model complexes.[25,28] Complex **3** has a symmetric structure with two $Fe_2S_2$ units linked to the opposite sites of the benzene ring. The four S atoms are located approximately in a plane with the benzene ring, which is a vertical plane of symmetry in the molecule of **3**. Complex **4**, a position isomer of **3**, has an eccentric structure with two vicinal $Fe_2S_2(CO)_6$ units fused to a benzene ring. The bond lengths and angles of complexes **3** and **4** are similar to those of **1**.[25] The distances of the Fe−Fe bonds are 2.4798(11) Å for **3** and 2.4893(9) and 2.4885(8) for **4**, which are shorter than that (2.5103(11) Å) in the well-known diiron complex ($\mu$-pdt)$[Fe_2(CO)_6]$.[29]

The molecule of **5** has two different units, $Fe_2(CO)_6$ and $Fe_2(CO)_5PPyr_3$, attached to opposite sides of the


dx.doi.org/10.1021/ic301647u | *Inorg. Chem.* 2013, 52, 1798−1806

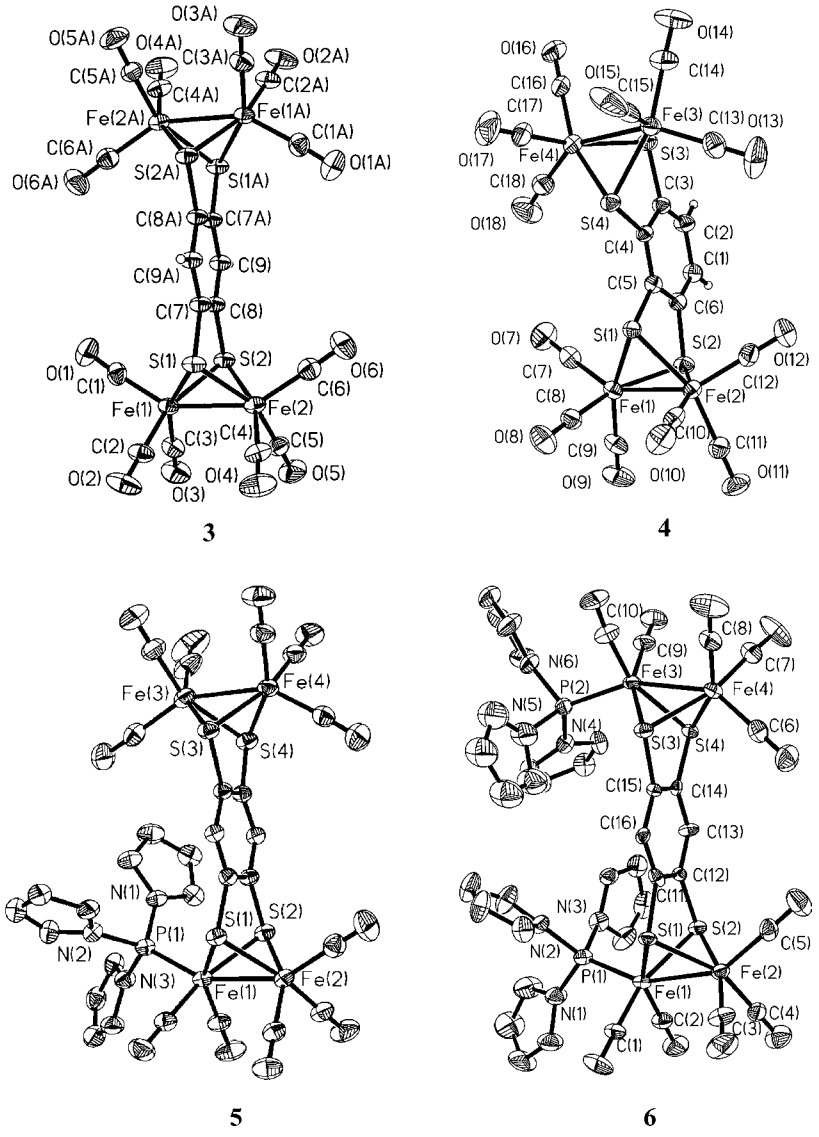


**Figure 3.** Molecular structures of **3**–**6** with thermal ellipsoids drawn at the 30% probability level. Hydrogen atoms have been omitted in the structures of **5** and **6** for clarity.

**Table 1. Selected Bond Lengths (Angstroms) and Angles (degrees) for 3–6**

| | 3 | 4 | 5 | 6 |
|---|---|---|---|---|
| bond lengths | | | | |
| Fe(1)–Fe(2) | 2.4798(11) | 2.4893(9) | 2.4873(5) | 2.492(3) |
| Fe(3)–Fe(4) | 2.4798(11) | 2.4885(8) | 2.4715(6) | 2.493(3) |
| Fe(1)–S(1) | 2.2705(13) | 2.2747(12) | 2.2865(7) | 2.280(3) |
| Fe(1)–S(2) | 2.2726(13) | 2.2626(12) | 2.2816(7) | 2.292(3) |
| Fe(1)–P(1) | | | 2.1814(7) | 2.193(4) |
| Fe(3)–P(2) | | | | 2.184(4) |
| Fe(1)–$C_{ba}$ | 1.794(6) | 1.778(5) | 1.774(3) | 1.803(16) |
| S(1)···S(2) | 2.9514(2) | 2.9504(2) | 2.9358(0) | 2.9457(6) |
| bond angles | | | | |
| S(1)–Fe(1)–S(2) | 81.03(5) | 81.22(4) | 79.97(2) | 80.5212(2) |
| Fe(1)–S(1)–Fe(2) | 66.18(4) | 66.39(3) | 66.08(2) | 66.35(10) |
| Fe(1)–S(2)–Fe(2) | 66.21(4) | 66.69(4) | 66.35(2) | 66.01(9) |
| S(1)–Fe(1)–Fe(2) | 56.93(4) | 56.75(3) | 56.75(2) | 56.72(9) |

benzenetetrathiolate bridge. The $PPyr_3$ ligand is in the apical position of one of the $Fe_2S_2$ units of **5**, just as other reported $Fe_2S_2$ complexes with bulky phosphine and phosphite ligands.[26,27] The distance of the Fe–Fe bond (2.4870(7) Å) in the $Fe_2(CO)_5PPyr_3$ unit of **5** is slightly longer than that (2.4798(11) Å) in the $Fe_2(CO)_6$ unit of **3**.


dx.doi.org/10.1021/ic301647u | Inorg. Chem. 2013, 52, 1798–1806

The IR and $^{1}H$ and $^{31}P$ NMR spectra of **6** suggest that it has two $Fe_2(CO)_5PPyr_3$ units connecting to both sides of the benzenetetrathiolate bridge, and furthermore, it can be deduced that the two bulky $PPyr_3$ ligands in complex **6** are located in the apical positions of two $Fe_2(CO)_5PPyr_3$ units in light of the structures of ($\mu$-$CH_3$bdt)[$Fe(CO)_3$][$Fe(CO)_2PPh_3$] ($CH_3$bdt = 4-methylbenzene-1,2-dithiolato) and ($\mu$-pdt)[$Fe(CO)_3$][$Fe(CO)_2$L] (L = $PPh_3$, $PMe_2Ph$).[26,28] However, we cannot determine whether the two $PPyr_3$ ligands are located in the same flank (configuration **A**) or different flanks (configuration **B**) of the plane formed by a benzene ring and four S atoms (Figure 4). Considering that the ligands would be less crowded

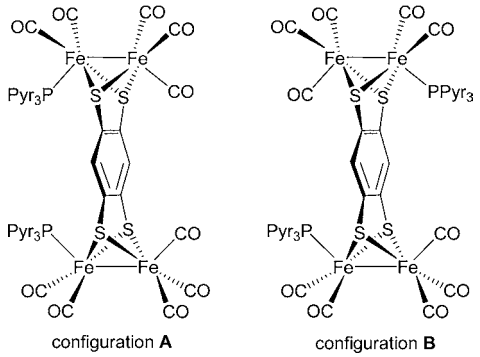


**Figure 4.** Possible configurations of the $PPyr_3$-disubstituted complex **6**.

in the molecule of **6** if the bulky $PPyr_3$ ligands were located at the apical positions of different flanks of the $S_2C_6H_2S_2$ plane, we predicted that the molecular structure of **6** is in configuration **B** with $C_{2h}$ symmetry. To our surprise, the single-crystal X-ray analysis reveals that complex **6** possesses $C_{2v}$ symmetry with two $PPyr_3$ ligands located at the apical positions of the same flank of the $S_2C_6H_2S_2$ plane, that is, configuration **A** in Figure 4. Accordingly, the two $Fe_2S_2$ units are pushed to the $Fe(CO)_3$ side due to the congestion of the two apical $PPyr_3$ ligands in the same flank of **6**. The dihedral angle between the planes of S(1)−Fe(1)−S(2) and S(1)−C(11)−C(12)−S(2) is 138.45°, which is apparently larger than that (130.1°) between the planes of S(1)−Fe(2)−S(2) and S(1)−C(11)−C(12)−S(2). Similarly, the dihedral angle (139.54°) between the planes of S(3)−Fe(3)−S(4) and S(3)−C(15)−C(14)−S(4) is much larger than that (129.25°) between the planes of S(3)−Fe(4)−S(4) and S(3)−C(15)−C(14)−S(4). The Fe−Fe bonds (2.492(3) and 2.493(3) Å) of **6** are longer than those in analogous complexes **3** and **5**.

**Cyclic Voltammograms of 3−6.** The redox potentials of structural and functional mimics of FeFe-hydrogenases are one of the important features for their application in electro- and photochemical hydrogen production. Cyclic voltammetry (CV) measurements were carried out in $CH_2Cl_2$ because of the solubility problem of these complexes in $CH_3CN$. CVs were scanned in the cathodic direction at a rate of 100 mV $s^{-1}$. All reduction potentials in Table 2 are given using ferrocene as an internal reference unless otherwise noted.

The all-carbonyl iron complexes **3** and **4** display essentially identical CVs (Figure 5 and Figure S1, Supporting Information). Each complex exhibits two chemically reversible reduction waves in $CH_2Cl_2$. The first reduction takes place at $E_{1/2}^{red1}$ = −1.38 V for **3** and −1.40 V for **4**, which is 40−60 mV less negative than that for the corresponding $Fe_2S_2$ complex **1** ($E_{1/2}$ = −1.44 V)[18] and 340−360 mV less negative than that for ($\mu$-pdt)[$Fe_2(CO)_6$],[17]

**Table 2. Reduction Potentials of 3−6 and Related $Fe_2S_2$ Complexes in $CH_2Cl_2$**

| complex | $E_{1/2}^{red1}$ (V) vs $Fc^+$/Fc | $E_{1/2}^{red2}$ (V) vs $Fc^+$/Fc |
|---|---|---|
| **3** | −1.38 (2e$^-$) | −1.66 (2e$^-$) |
| **4** | −1.40 (2e$^-$) | −1.66 (2e$^-$) |
| **5** | −1.42 (2e$^-$) | −1.70 (2e$^-$) |
| **6** | −1.47 (2e$^-$) | −1.79 (2e$^-$) |
| **1**[a] | −1.44 (2e$^-$) | |
| ($\mu$-pdt)[$Fe_2(CO)_6$] | −1.74 (e$^-$)[b] | −2.35 (e$^-$)[b] |

[a]Reference 18. [b]$E_{pc}$ in $CH_3CN$, ref 17.

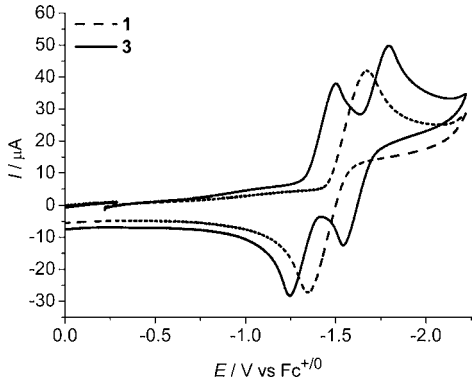


**Figure 5.** CVs of **3** and **1** (1.0 mM) in $n$$Bu_4NPF_6$/$CH_2Cl_2$.

because the electrons in the molecules of **3** and **4** are delocalized over two $Fe_2S_2(CO)_6$ units through the benzene bridge. The second reductions of **3** and **4** occur at the same potential ($E_{1/2}^{red2}$ = −1.66 V). The good chemical reversibility of the reduction events at the CV time scale is evidenced by the peak current ratio $i_{pa2}/i_{pc1}$ (~0.96 for **3** and ~1.0 for **4**), indicating the strong stabilization of reduced species of **3** and **4** by the conjugate and rigid benzene bridge.

It was reported that ($\mu$-bdt)[$Fe_2(CO)_6$] (**1**) displayed a reversible reduction wave for a two-electron process.[18−20] We demonstrated that the two reduction waves of **3** each represent a two-electron event by bulk electrolysis of a $CH_2Cl_2$ solution of **3** and splitting of the first reduction wave in THF (Figure S2, Supporting Information).[30] Therefore, the first reduction peak in $CH_2Cl_2$ is attributed to the couple of $\mathbf{3}/\mathbf{3}^{2-}$ and the second one to $\mathbf{3}^{2-}/\mathbf{3}^{4-}$. It is the same for the reduction process of **4**. The differences ($\Delta E = E_{1/2}^{red1} - E_{1/2}^{red2}$) in the first and second reduction potentials in $CH_2Cl_2$ are about 280 mV for **3** and 270 mV for **4**. The small differences in potential values suggest that the first two-electron reduction occurs at one of the $Fe_2S_2$ units and after first reduction, the reduced $[Fe_2(CO)_6]^{2-}$ unit increases the electron richness of the other $Fe_2(CO)_6$ unit, indicating that there exists an electronic communication among the iron centers of the two $Fe_2S_2$ units through the benzene plane in **3** and **4**. All results obtained from the electrochemical studies show that **3** and **4** can act as four-electron transformation templates in two reversible two-electron events.

The two reduction waves of the all-carbonyl complex **3** become less chemically reversible for $PPyr_3$-mono- and -disubstituted complexes **5** and **6** in $CH_2Cl_2$ (Figure S3, Supporting Information). A similar loss of reversibility was observed for mono- and disubstituted derivatives of **1**.[31,32] The two reduction waves of **5** appear at −1.42 ($E_{1/2}^{red1}$) and −1.70 V ($E_{1/2}^{red2}$), showing a shift to the cathodic direction by 40 mV as compared to the corresponding potentials of the all-carbonyl iron complex **3**.


dx.doi.org/10.1021/ic301647u | Inorg. Chem. 2013, 52, 1798−1806

The two reduction waves of the $PPyr_3$-disubstituted complex **6** are further negatively shifted to −1.47 ($E_{1/2}^{red1}$) and −1.79 V ($E_{1/2}^{red2}$). The small negative shifts of the reduction potentials resulting from CO displacement of **3** by $PPyr_3$ are consistent with the weaker electron donor character of $PPyr_3$ as compared to trialkylphosphines and $PPh_3$. On the basis of these results, the first reduction waves of **5** and **6** are assigned to the processes of **5** to $\mathbf{5}^{2-}$ and **6** to $\mathbf{6}^{2-}$ species, respectively, and the second one to the further two-electron reduction of $\mathbf{5}^{2-}$ to $\mathbf{5}^{4-}$ and $\mathbf{6}^{2-}$ to $\mathbf{6}^{4-}$ species.

**Electrocatalytic Reduction of Protons from Acetic Acid and Its Derivatives with 3−6 as Catalysts.** Complexes **3**−**6** were investigated as electrocatalysts for reduction of protons from organic acids, such as $CH_3COOH$, $CH_2ClCOOH$, $CHCl_2COOH$, $CCl_3COOH$, and $CF_3COOH$. The current heights of the reduction peaks of **3** did not go up with an increase of the concentration of $CH_3COOH$ in $CH_2Cl_2$ (Figure 6).

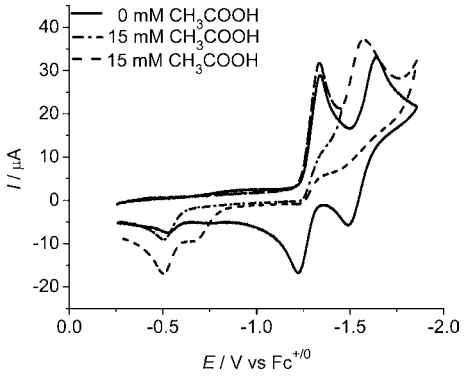


**Figure 6.** CVs of **3** (0.75 mM) in $n$Bu$_4$NPF$_6$/$CH_2Cl_2$ in the absence of acid (solid line), addition of 15 equiv of $CH_3COOH$ to the solution, and with scan reversed at −1.45 (dash-dotted line) and −1.85 V (dashed line).

A new reduction wave at $E_p^{red}$ = −1.57 V and two new anodic waves at $E_p^{ox}$ = −0.51 and −0.66 V appeared in the CV of **3**, while the reduction waves of **3** became irreversible. Similar changes were observed in the CV of **4** upon addition of $CH_3COOH$ (Figure S4, Supporting Information). With addition of $CH_3COOH$, the apparent decrease in the current height of $\mathbf{3}^{2-}$/**3** oxidation wave may result from protonation of the reduced species $\mathbf{3}^{2-}$, most certainly to form $\mathbf{3H}^-$. The IR spectrum of $\mathbf{3}^{2-}$ recorded during reduction of **3** at a controlled potential of −0.9 V vs Ag/AgCl or in the presence of 2 equiv of $Cp^*_2Co$ shows six CO bands at 2067, 2034, 1991 1971, 1930, and 1884 $cm^{-1}$ (Figures S5 and S6, Supporting Information), indicating that the two-electron reduction occurs at one of the $Fe_2S_2$ units of **3** to form a $[(Fe^0Fe^0)(Fe^IFe^I)]^{2-}$ species.[30] After chemical reduction of **3**, subsequent protonation of $\mathbf{3}^{2-}$ upon addition of $CH_3COOH$ occurs at the $Fe^0Fe^0$ unit, resulting in formation of the $[(Fe^IHFe^I)(Fe^IFe^I)]^-$ and/or $[(Fe^0Fe^{II}H)(Fe^IFe^I)]^-$ intermediate ($\mathbf{3H}^-$).[23,20] The strengths of low-wavenumber CO bands of $\mathbf{3}^{2-}$ attributed to the $Fe^0Fe^0$ unit apparently decreased, and all CO bands shifted by 4−8 $cm^{-1}$ to higher wavenumbers. Quantitative recovery of the absorptions of **3** is observed in the react-IR spectra upon addition of 1.5 equiv of $CF_3COOH$ to the $\mathbf{3H}^-$ solution, implicating generation of $H_2$ by combination of a proton with the hydride of $\mathbf{3H}^-$.

The structure of $\mathbf{3H}^-$ was investigated by $^1$H NMR spectroscopy. A 2 equiv amount of $Cp^*_2Co$ was added to the THF-$d_8$ solution of **3** (10 mM) in an NMR test tube under Ar atmosphere. After the color of the solution changed from red to dark green, 4 equiv of $CH_3COOH$ was immediately added. The sample was measured instantly at 20 °C (Figure S7, Supporting Information). The signals at $\delta$ 7.40 and 6.89 are attributed to the two protons in the benzene ring of the reduced and protonated species $\mathbf{3H}^-$. It is noteworthy that tetranuclear iron complex **3** displays only one signal at $\delta$ 6.98 for the two protons at ortho positions of the benzene ring, while $\mathbf{3H}^-$ exhibits a signal for each proton, implicating that the symmetric structure of **3** changes to an unsymmetric structure with cleavage of one of the Fe−S bonds in the reduced and protonated $Fe_2S_2$ moiety of $\mathbf{3H}^-$.[20] In the high field, only one signal was observed at $\delta$ −8.96, which is in accordance with the chemical shift of the $\mu$-hydride ($\delta$ −8.79) in the $[\mathbf{1}(\mu\text{-H})]^-$ species suggested by Tilley and co-workers.[33] $^1$H NMR and DFT studies on the $\mathbf{1H}^-$ suggest that protonation of $\mathbf{1}^{2-}$ affords $[Fe^IHFe^I]^-$ as the major species of $\mathbf{1H}^-$ and $[Fe^0Fe^{II}H]^-$ as the minor species. However, the $^1$H NMR signal of the terminal hydride of $[(Fe^0Fe^{II}H)(Fe^IFe^I)]^-$ species is not detected for $\mathbf{3H}^-$ that is measured under identical conditions as $\mathbf{1H}^-$ ($\delta$(terminal hydride) −11.69 for the $[Fe^0Fe^{II}H]^-$ species derived from **1**). All $^1$H NMR evidence supports formation of the $[(Fe^IHFe^I)(Fe^IFe^I)]^-$ species when **3** is successively reduced and protonated. Considering the structural similarity of **3** and **1**, we assume that the $[Fe^IHFe^I]^-$ moiety of $\mathbf{3H}^-$ has a similar structure as $[\mathbf{1}(\mu\text{-H})]^-$ (Figure S7, Supporting Information).[33]

The electrocatalytic property of **1** for proton reduction in the presence of acids with different strength, such as $HBF_4$ ($pK_a \approx 2$),[18] HOTs ($pK_a \approx 8.7$),[34] and $CH_3COOH$ ($pK_a \approx 22.3$),[34] has been well studied (all $pK_a$ values are given in $CH_3CN$). It is reported that a new anodic wave appeared at about −0.5 V in the CV of **1** on the reverse scan in the presence of $HBF_4$, HOTs, or $CH_3COOH$. This anodic wave is attributed to oxidation of $\mathbf{1H}^-$, formed by protonation of the reduced species $\mathbf{1}^{2-}$.[19] Accordingly, the new anodic wave detected at −0.51 V on the reverse scan in the CV of **3** is ascribed to oxidation of the protonated species of $\mathbf{3}^{2-}$. As $\mathbf{3}^{2-}$ is readily protonated in the presence of excess $CH_3COOH$, the cathodic wave at −1.57 V corresponds to reduction of $\mathbf{3H}^-$ to $\mathbf{3H}^{3-}$, which is immediately protonated to form $\mathbf{3}(H,H)^{2-}$. It is noted that the oxidative wave at −0.66 V does not appear when the scan range is limited to −1.45 V. Therefore, the anodic wave at −0.66 V is ascribed to oxidation of the doubly protonated species $\mathbf{3}(H,H)^{2-}$, formed by reduction of $\mathbf{3H}^-$ at −1.57 V and subsequent protonation of $\mathbf{3H}^{3-}$ (Figure 6, Scheme 1). Despite formation of a doubly protonated species, the primary reduction of **3** occurs at a potential that is too mild to electrochemically catalyze the proton reduction in the presence of $CH_3COOH$, just as that reported for complex **1**.[18−21] Although the reduction potentials of phosphine-substituted complexes **5** and **6** are 40−130 mV

**Scheme 1. Plausible Reactions of the Reduced Species of 3 in the Presence of $CH_3COOH$**

$$\mathbf{3} + 2e^- \Leftrightarrow \mathbf{3}^{2-}\ (E_{1/2}^{red1} = -1.38\ \text{V})$$

$$\mathbf{3}^{2-} + H^+ \rightarrow \mathbf{3H}^-$$

$$\mathbf{3H}^- \Leftrightarrow \mathbf{3H} + e^-\ (E_p^{ox} = -0.51\ \text{V})$$

$$\mathbf{3H}^- + 2e^- \Leftrightarrow \mathbf{3H}^{3-}\ (E_p^{red} = -1.57\ \text{V})$$

$$\mathbf{3H}^{3-} + H^- \rightarrow \mathbf{3}(H,H)^{2-}$$

$$\mathbf{3}(H,H)^{2-} \Leftrightarrow \mathbf{3}(H,H)^- + e^-\ (E_p^{ox} = -0.66\ \text{V})$$


dx.doi.org/10.1021/ic301647u | Inorg. Chem. 2013, 52, 1798−1806

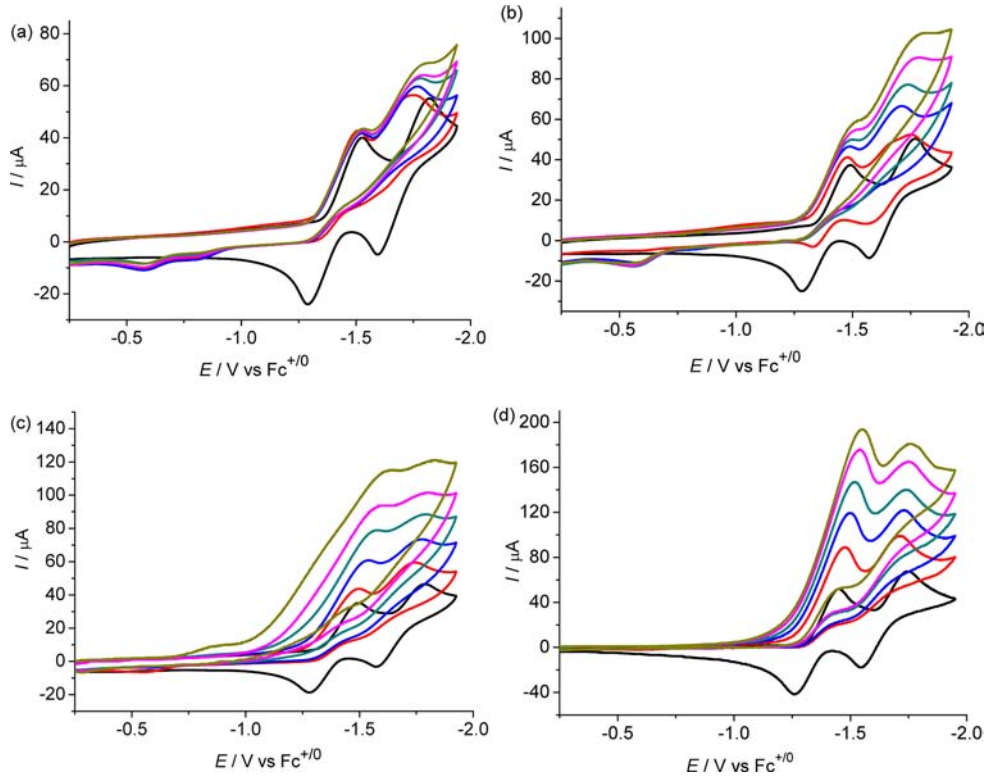


**Figure 7.** CVs of **3** (1.0 mM) with addition of 0−10 mM (a) $CH_2ClCOOH$, (b) $CHCl_2COOH$, (c) $CCl_3COOH$, and (d) $CF_3COOH$ to the solution of **3** in $CH_2Cl_2$ containing 0.05 M $n$Bu$_4$NPF$_6$.

more negative than the all-CO complexes **3** and **4**, the increase in basicity provided by CO substitution, which parallels the change in reduction potential, is not sufficient to trigger catalysis of electrochemical proton reduction in the presence of $CH_3COOH$ (Figure S8, Supporting Information).

Similarly, two irreversible waves and two new anodic waves were observed upon addition of $CH_2ClCOOH$ ($pK_a \approx 15.3$)[34] to the $CH_2Cl_2$ solution of **3** (Figure 7a). It is noteworthy that oxidation of $\mathbf{3}^{2-}$ was completely suppressed upon addition of 2 mol equiv of $CH_2ClCOOH$. However, the current height and position of the first reduction wave did not show any considerable change. Upon addition of excess chloroacetic acid (10 mM), the position of the second reduction wave positively shifted from −1.81 ($E_{pc}$) to −1.74 V, but its intensity did not apparently increase ($i_c/i_p$ = 1.3, the ratio of the current after ($i_c$) to that before ($i_p$) addition of acid is used to measure the extent of proton reduction catalysis), suggesting no or very slow catalytic reduction of protons upon reduction of the $\mathbf{3H}^-$ intermediate. Similarly, the second reduction peak of **4** increased marginally by a factor of $i_c/i_p$ = 1.2 upon addition of 10 mol equiv of $CH_2ClCOOH$ (Figure S9, Supporting Information). In contrast, no considerable increase of the reduction wave of **1** was observed when the concentration of chloroacetic acid was increased to 10 mM (Figure S10, Supporting Information) as described in the literature.[20]

CVs recorded upon addition of 0−10 mM $CHCl_2COOH$ ($pK_a \approx 13.2$) or $CCl_3COOH$ ($pK_a \approx 10.6$)[34] to a $CH_2Cl_2$ solution of **3** (1.0 mM) are shown in Figure 7b and 7c, respectively. Upon addition of 10 mol equiv of $CHCl_2COOH$, the height of the first reduction wave is increased by a factor of $i_c/i_p$ = 1.4 ($\Delta I$ = 25 $\mu$A) and the height of the second reduction wave by a factor of 2.5 ($\Delta I$ > 50 $\mu$A, Figure 7b). This voltammetric response is consistent with proton reduction catalysis occurring mainly at the potential of the reduction of $\mathbf{3H}^-$. With addition of $CCl_3COOH$ up to 10 mM, the first reduction wave is increased by a factor $i_c/i_p$ = 3.0 ($\Delta I$ = 80 $\mu$A), while the intensity increase of the second reduction wave is almost suppressed (Figure 7c). In the presence of comparatively strong acid, catalysis occurs mainly at the potential of the $\mathbf{3}/\mathbf{3}^{2-}$ couple, as previously observed for **1**.[18,19]

In addition to chloro-substituted acetic acids, we also investigated the electrocatalytic property of **3**−**6** for reduction of protons from $CF_3COOH$ ($pK_a \approx 12.7$)[34] and compared the results with **1**. The CVs for a 1.0 mM solution of **3** with 0−10 mM $CF_3COOH$ are shown in Figure 7d. Catalysis occurs at the potential of the first reduction peak at −1.38 V, as seen with trichloroacetic acid as a proton source. A current enhancement $i_c/i_p$ = 3.6 was achieved upon addition of $CF_3COOH$ up to 10 mM. Complex **4** displays similar CV features (Figure S11, Supporting Information) as those observed for **3** (Figure 7d). The height of the first reduction wave of **4** is increased by a factor of $i_c/i_p$ = 2.9 upon addition of 10 mol equiv of $CF_3COOH$. For mono- and diphosphine-substituted tetranuclear iron complexes **5** and **6**, catalysis also occurs at the potential of the first reduction waves reaching a value of $i_c/i_p \approx 5$ in the presence of 10 mM $CF_3COOH$ (Figure S12, Supporting Information). In contrast, the catalytic peak of **1** is only raised by a factor of $i_c/i_p$ = 2.5 ($\Delta I$ = 70 $\mu$A) under the same conditions (Figure S13, Supporting Information). The peak current of the first reduction waves of **3**−**6** varies linearly with the concentration of $CF_3COOH$ in the range 0−10 mM, indicating a second-order dependence of the catalytic rate on acid (Figure 8 and Figure S14, Supporting Information). The steeper slopes observed for **3** and **4** relative to that for **1** indicate an increased catalytic activity of the two tetra-iron derivatives.

It is found that the current heights of the two new anodic waves in the range from −0.5 to −0.7 V observed on the


dx.doi.org/10.1021/ic301647u | Inorg. Chem. 2013, 52, 1798−1806

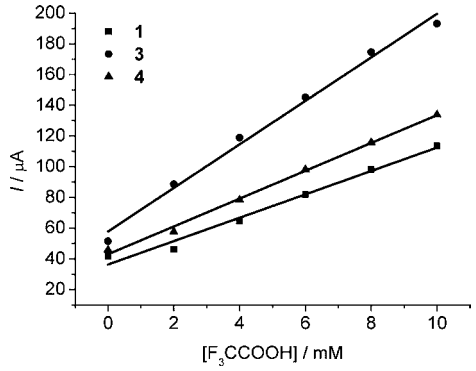


**Figure 8.** Dependence of the first catalytic peak currents for 1.0 mM **1**, **3**, and **4** on the concentration of $CF_3COOH$ in $CH_2Cl_2$.

reverse scan in Figure 6 gradually decrease as the acid strength is increased. The similar phenomenon was also observed for complex **1** with an increase of the concentration of HOTs.[19] It is noteworthy that the two anodic peaks observed on the reverse scan in Figures 6 and 7a–c completely disappear in Figure 7d, suggesting that the oxidations of the $3H^-$ and $3(HH)^{2-}$ is significantly suppressed in the presence of $CF_3COOH$. An increase of the acid strength is capable of facilitating the further reactions of the iron–hydride anions with protons to generate hydrogen, that is, $3H^- + H^+ \rightarrow H_2 + 3$ and $3(HH)^{2-} + H^+ \rightarrow H_2 + 3H^-$.

On the basis of the results obtained from the electrochemical experiments and the previously reported mechanism for electrocatalytic proton reduction by complex **1**,[19,20] the mechanisms for electrocatalytic hydrogen production with **3** are proposed in Scheme 2, which includes two ECC catalytic cycles.

**Scheme 2. Proposed Mechanism for Electrocatalytic $H_2$ Production with 3 as Catalyst**

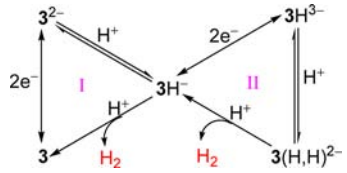


The $pK_a$ of the acid adopted greatly influences the pathways of electrochemical reactions of **3**. In the presence of $CH_3COOH$, complex **3** is not catalytically active for proton reduction to hydrogen because the reduced and protonated species $3H^-$ and $3(H,H)^{2-}$ could not directly react with protons from this weak acid and the oxidation reactions of $3H^-$ and $3(H,H)^{2-}$ are detected on the reverse scan. With $CH_2ClCOOH$ as the proton source, the $3/3^{2-}$ couple is catalytically inactive while the reduction of $3H^-$ triggers catalysis via path II, indicating that $CH_2ClCOOH$ is capable of protonating $3(H,H)^{2-}$. From the $pK_a$ of acetic and chloroacetic acid in acetonitrile, we can roughly estimate the $pK_a$ value of $3(H,H)^{2-}$ as between 15.3 and 22.3. Similarly, we can estimate that the $pK_a$ value of $3H^-$ is in the range of 13–15. Using these data and a thermodynamic cycle similar to that proposed by DuBois and co-workers,[35] the hydride donor ability of $3H^-$ could be estimated to be in the order of $\Delta G^0{}_{H^-} \approx 35$ kcal mol$^{-1}$. This is a rough estimate since our measurements were carried out in dichloromethane rather than acetonitrile (see the Supporting Information).

Upon addition of $CHCl_2COOH$ to the $CH_2Cl_2$ solution of **3**, proton reduction occurs via both catalytic cycles I and II, suggesting that the $CHCl_2COOH$ is strong enough to protonate $3H^-$ and $3(H,H)^{2-}$. The variation of the peak height with acid concentration suggests that catalytic path II is kinetically favored over path I in the presence of $CHCl_2COOH$. Proton reduction catalysis occurs mainly through path I in the presence of a stronger acid such as $CCl_3COOH$ and $CF_3COOH$ because $3H^-$ is rapidly protonated. A cleaner electrocatalytic proton reduction process was observed with **3** using $CF_3COOH$ as proton source, although the $pK_a$ value of this acid in acetonitrile (~12.5) is slightly higher than that of trichloroacetic acid (~10.5). This dependence of the electrocatalytic rate on the acid type might be explained here by a better match of the $pK_a$ of $CF_3COOH$ with that of the reduced protonated form $3H^-$ and/or better access of $CF_3COOH$ close to the hydride position in $3H^-$.[36]

## CONCLUSIONS

Tetranuclear iron–sulfur complexes **3**–**6**, with two $Fe_2S_2$ units linked by a rigid and conjugate benzene bridge, are four-electron transfer relays via two consecutive reversible two-electron reduction events, and their reduced species are stabilized by delocalization of negative charges over the conjugate system. Such biomimics of the FeFe-hydrogenase active site are promising catalysts for four-electron reduction of substrates. The $Fe_4S_4$ complexes **3** and **4** display different catalytic behaviors from the $Fe_2S_2$ complex **1** for electrochemical reduction of protons from $CH_2ClCOOH$. The catalytic peaks of **3** and **4** appear at $E_{pc} = -1.74$ and $-1.65$ V, respectively, while complex **1** is electrocatalytically inactive at the potential more positive than $-1.8$ V under the same conditions.[20] Two ECC pathways for electrocatalytic reduction of protons by **3** are proposed. The second pathway with $3(HH)^{2-}$ as a key intermediate is dominant for electrochemical hydrogen production in the presence of weaker organic acids, $CH_2ClCOOH$ and $CHCl_2COOH$, while the first pathway with $3H^-$ as a curtail intermediate becomes an important pathway in the presence of stronger acids, $CCl_3COOH$ and $CF_3COOH$. Among the organic acids being tested, $CF_3COOH$ is the best acid for electrochemical proton reduction catalyzed by **3**, with almost quantitative regeneration of **3** from $3H^-$ and $3H^-$ from $3(HH)^{2-}$ in the catalytic cycle, likely because of a better match of the $pK_a$ of this acid with that of the reduced protonated form $3H^-$ and/or better access close to the hydride position in $3H^-$. Further studies on the details of the mechanism for the $H_2$-evolving reaction catalyzed by **3** are under way.

## EXPERIMENTAL SECTION

**Reagents and Instruments.** All reactions and operations related to organometallic complexes were carried out under dry oxygen-free dinitrogen with standard Schlenk techniques. Solvents were dried and distilled prior to use according to standard methods. 1,2,4,5- and 1,2,3,4-Tetrachlorobenzene reagents were purchased from Fluka, and isopropanethiol was purchsed from Acros. Other commercially available chemicals such as $Fe(CO)_5$ and pyrrole were purchased from local suppliers and used as received. Compounds $Fe_3(CO)_{12}$,[37] 1,2,4,5- and 1,2,3,4-tetramercaptobenzene,[38] and tris(*N*-pyrrolyl)-phosphine[39] were prepared according to literature procedures. Complexes **1** and **2** were prepared according to literature procedures.[21,25]

Infrared spectra were recorded in KBr discs with a JASCO FT/IR 430 spectrophotometer. Proton and $^{31}P\{^1H\}$ NMR spectra were collected with a Varian INOVA 400 NMR spectrometer. Mass spectra were recorded on an ESI-Q-TOF MS (Micro) instrument. Elemental


dx.doi.org/10.1021/ic301647u | Inorg. Chem. 2013, 52, 1798–1806

analyses were performed with a Thermoquest-Flash EA 1112 elemental analyzer.

**Synthesis of ($\mu,\mu$-pbtt)[$Fe_2(CO)_6$]$_2$ (3).** Compound 1,2,4,5-tetramercaptobenzene (1.0 g, 5.0 mmol) was added to the solution of $Fe_3(CO)_{12}$ (6.04 g, 12.0 mmol) in THF (100 mL). The mixture was stirred at 70 °C overnight. The resulting solution was evaporated to dryness under reduced pressure. The residue was purified by column chromatography on neutral alumina with hexane as eluent. Pure complex **3** was obtained as red crystals after recrystallization in hexane at −30 °C. Yield: 2.36 g (62%). IR (KBr, $cm^{-1}$): $\nu$(CO) 2078 (m), 2036 (s), 2003 (vs), 1981 (m). $^1$H NMR (400 MHz, $CDCl_3$): $\delta$ 6.87 (s, 2H, $C_6H_2$). TOF-ESI-MS. Calcd for $[M]^+$: $m/z$ 761.5827. Found: $m/z$ 761.5863.

**Synthesis of ($\mu,\mu$-obtt)[$Fe_2(CO)_6$]$_2$ (4).** Compound 1,2,3,4-tetramercaptobenzene (1.03 g, 5.0 mmol) was added to the solution of $Fe_3(CO)_{12}$ (6.04 g, 12.0 mmol) in toluene (100 mL). The mixture was stirred at reflux for 2 h. The resulting solution was evaporated to dryness under reduced pressure. The residue was purified by column chromatography on silica gel with hexane as eluent. Pure complex **4** was obtained as red crystals after recrystallization in hexane at room temperature. Yield: 1.2 g (32%). IR ($CH_2Cl_2$, $cm^{-1}$): $\nu$(CO) 2075 (m), 2049 (s), 2003 (vs). $^1$H NMR (400 MHz, $CDCl_3$): $\delta$ 6.43 (s, 2H, $C_6H_2$). TOF-ESI-MS. Calcd for $[M]^+$: $m/z$ 761.5827. Found: $m/z$ 733.5926 $[M-CO]^+$.

**Synthesis of ($\mu,\mu$-pbtt)[$Fe_2(CO)_6$][$Fe_2(CO)_5(PPyr_3)$] (5).** Complex **3** (1.0 g, 1.31 mmol) and tris(*N*-pyrrolyl)phosphine (0.3 g, 1.31 mmol) were dissolved in toluene (80 mL). The mixture was refluxed for 72 h under $N_2$ atmosphere. The resulting solution was evaporated to dryness under reduced pressure. The dark red crude product was purified by column chromatography on silica gel with dichloromethane/hexane (1:10, v/v) as eluent. Pure complex **5** was obtained as red crystals after recrystallization in a mixed solvent of dichloromethane/pentane at −30 °C. Yield: 0.8 g (63%). IR (KBr, $cm^{-1}$): $\nu$(CO) 2078 (m), 2058 (s), 2043 (s), 2002 (vs), 1986 (m), 1960 (m). $^1$H NMR (400 MHz, $CDCl_3$): $\delta$ 6.40 (s, 6H, Pyr), 6.64 (s, 2H, $C_6H_2$), 6.90 (s, 6H, Pyr). $^{31}$P{$^1$H} NMR ($CDCl_3$): $\delta$ 139.72. Anal. Calcd for $C_{29}H_{14}Fe_4N_3O_{11}PS_4$: C, 36.17; H, 1.47; N, 4.36. Found: C, 35.97; H, 1.54; N, 4.40.

**Synthesis of ($\mu,\mu$-pbtt)[$Fe_2(CO)_5(PPyr_3)$]$_2$ (6).** Complex **3** (1.0 g, 1.31 mmol) and tris(*N*-pyrrolyl)phosphine (0.6 g, 2.62 mmol) were dissolved in toluene (80 mL). The mixture was refluxed for 72 h under $N_2$ atmosphere. TLC analysis showed that there were small amounts of unreacted complex **3** and $PPyr_3$-monosubstituted complex **5**. The resulting solution was evaporated to dryness under reduced pressure. The dark red crude product was purified by column chromatography on silica gel, first with hexane as eluent to remove complex **3**, then with dichloromethane/hexane (1:10, v/v) as eluent to isolate complex **5**, and finally with dichloromethane/hexane (1:4, v/v) as eluent to get the $PPyr_3$-disubstituted product **6**. Pure complex **6** was obtained as an orange crystalline solid after recrystallization in a mixed solvent of dichloromethane/pentane at −30 °C. Yield: 0.63 g (41%). IR (KBr, $cm^{-1}$): $\nu$(CO) 2057 (s), 2008 (s), 1983 (s), 1963 (m). $^1$H NMR (400 MHz, $CDCl_3$): $\delta$ 6.40 (s, 12H, Pyr), 6.62 (s, 2H, $C_6H_2$), 6.94 (s, 12H, Pyr). $^{31}$P{$^1$H} NMR ($CDCl_3$): $\delta$ 137.54. Anal. Calcd for $C_{40}H_{26}Fe_4N_6O_{10}P_2S_4$: C, 41.26; H, 2.25; N, 7.22. Found: C, 41.05; H, 2.33; N, 7.15.

**X-ray Structure Determination of 3−6.** Single-crystal X-ray diffraction data were collected with an Bruker Smart Apex II CCD diffractometer with graphite-monochromated Mo K$\alpha$ radiation ($\lambda$ = 0.071073 Å) at 298 K using the $\omega$−2$\theta$ scan mode. Data processing was accomplished with the SAINT processing program. Intensity data were corrected for absorption by the SADABS program. All structures were solved by direct methods and refined on $F^2$ against full-matrix least-squares methods using the SHELXTL 97 program package. All non-hydrogen atoms were refined anisotropically. Hydrogen atoms were located by geometrical calculation. Details of crystal data, data collections, and structure refinements are summarized in Table S1 (Supporting Information).

**Electrochemistry Studies of 3−6.** Dichloromethane (Aldrich, spectroscopy grade) used for electrochemical measurements was freshly distilled from $CaH_2$ under $N_2$. Cyclic voltammograms were obtained in a three-electrode cell under Ar using a BAS 100W electrochemical workstation. The working electrode was a glassy carbon disc (diameter 3 mm) polished with 3 and 1 $\mu$m diamond pastes and sonicated in ion-free water for 15 min prior to use. The reference electrode was a nonaqueous $Ag/Ag^+$ (0.01 M $AgNO_3$ in $CH_3CN$) electrode, and the counter electrode was platinum wire. The ferrocenium/ferrocene ($Fc^+$/Fc) couple was used as an internal reference, and all potentials given in this work are referred to the $Fc^+$/Fc potential. A solution of 0.05 M $n$Bu$_4$NPF$_6$ (Fluka, electrochemical grade) in $CH_2Cl_2$ was used as supporting electrolyte, which was degassed by bubbling with dry argon for 15 min before measurement. Bulk electrolysis was made using an EG&G potentiostat, model 273A, with a mercury electrode as working electrode (diameter 1 cm) and a platinum grid as auxiliary electrode. The Ag/AgCl/3.0 M KCl reference electrode was placed in a compartment separated from the working cell by a glass frit. Bulk electrolysis was made in a 0.3 M solution of $n$Bu$_4$NBF$_4$ in degassed $CH_2Cl_2$.

## ■ ASSOCIATED CONTENT

### Ⓢ Supporting Information

Cyclic voltammograms of **4**, **5**, and **6**, as well as cyclic voltammograms of **3** with $CH_3COOH$, crystallographic information files (CIF). This material is available free of charge via the Internet at http://pubs.acs.org.

## ■ AUTHOR INFORMATION

### Corresponding Author

*E-mail: symbueno@dlut.edu.cn.

### Notes

The authors declare no competing financial interest.

## ■ ACKNOWLEDGMENTS

We are grateful to the Natural Science Foundation of China (grant nos. 20633020 and 21120102036), the Basic Research Program of China (grant no. 2009CB220009), the Swedish Energy Agency, the Swedish Research Council, and the K&A Wallenberg Foundation for financial support of this work. We appreciate Prof. M. Fontecave, Dr. V. Artero, and P. D. Tran for their help in bulk electrolysis experiments and discussions.

## ■ REFERENCES

(1) Lovenberg, W. *Iron-Sulfur Proteins*; Academic Press: New York, 1973; Vols. *I* and *II*.
(2) Sprio, T. G. *Iron-Sulfur Proteins*; Wiley: New York, 1982.
(3) Cammack, R.; Skyes, A. G. *Iron−Sulfur Proteins*; Academic Press: San Diego, CA, 1992.
(4) Peters, J. W.; Lanzilotta, W. N.; Lemon, B. J.; Seefeldt, L. C. *Science* **1998**, *282*, 1853−1858.
(5) Benson, E. E.; Kubiak, C. P.; Sathrum, A. J.; Smieja, J. M. *Chem. Soc. Rev.* **2009**, *38*, 89−99.
(6) Tard, C.; Pickett, C. J. *Chem. Rev.* **2009**, *109*, 2245−2274.
(7) Gloaguen, F.; Rauchfuss, T. B. *Chem. Soc. Rev.* **2009**, *38*, 100−108.
(8) Liu, X.; Ibrahim, S. K.; Tard, C.; Pickett, C. J. *Coord. Chem. Rev.* **2005**, *249*, 1641−1652.
(9) Capon, J.-F.; Gloaguen, F.; Schollhammer, P.; Talarmin, J. *Coord. Chem. Rev.* **2005**, *249*, 1664−1676.
(10) Sun, L.; Åkermark, B.; Ott, S. *Coord. Chem. Rev.* **2005**, *249*, 1653−1663.
(11) Wang, M.; Sun, L. *ChemSusChem* **2010**, *3*, 551−554.
(12) Mejia-Rodriguez, R.; Chong, D.; Reibenspies, J. H.; Soriaga, M. P.; Darensbourg, M. Y. *J. Am. Chem. Soc.* **2004**, *126*, 12004−12014.
(13) Chong, D.; Georgakaki, I. P.; Mejia-Rodriguez, R.; Sanabria-Chinchilla, J.; Soriaga, M. P.; Darensbourg, M. Y. *Dalton. Trans.* **2003**, 4150−4163.

(14) Gloaguen, F.; Lawrence, J. D.; Schmidt, M.; Wilson, S. R.; Rauchfuss, T. B. *J. Am. Chem. Soc.* **2001**, *123*, 12518−12527.
(15) Capon, J.-F.; Gloaguen, F.; Pétillon, F. Y.; Schollhammer, P.; Talarmin, J. *Coord. Chem. Rev.* **2009**, *253*, 1476−1494.
(16) Zeng, X.; Li, Z.; Liu, X. *Electrochim. Acta* **2010**, *55*, 2179−2185.
(17) Liu, T.; Wang, M.; Shi, Z.; Cui, H.; Dong, W.; Chen, J.; Åkermark, B.; Sun, L. *Chem.—Eur. J.* **2004**, *10*, 4474−4479.
(18) Capon, J.-F.; Gloaguen, F.; Schollhammer, P.; Talarmin, J. *J. Electroanal. Chem.* **2004**, *566*, 241−247.
(19) Capon, J. F.; Gloaguen, F.; Schollhammer, P.; Talarmin, J. *J. Electroanal. Chem.* **2006**, *595*, 47−52.
(20) Felton, G. A. N.; Vannucci, A. K.; Chen, J.; Lockett, L. T.; Okumura, N.; Petro, B. J.; Zakai, U. I.; Evans, D. H.; Glass, R. S.; Lichtenberger, D. L. *J. Am. Chem. Soc.* **2007**, *129*, 12521−12530.
(21) Schwartz, L.; Singh, P. S.; Eriksson, L.; Lomoth, R.; Ott, S. *C. R. Chim.* **2008**, *11*, 875−889.
(22) Borg, S. J.; Behrsing, T.; Best, S. P.; Razavet, M.; Liu, X.; Pickett, C. J. *J. Am. Chem. Soc.* **2004**, *126*, 16988−16999.
(23) Quentel, F.; Passard, G.; Gloaguen, F. *Energy Environ. Sci.* **2012**, *5*, 7757−7761.
(24) Streich, D.; Astuti, Y.; Orlandi, M.; Schwartz, L.; Lomoth, R.; Hammarström, L.; Ott, S. *Chem.—Eur. J.* **2010**, *16*, 60−63.
(25) Cabeza, J. A.; Martínez-Carcía, M. A.; Riera, V. *Organometallics* **1998**, *17*, 1471−1477.
(26) Li, P.; Wang, M.; He, C.; Li, G.; Liu, X.; Chen, C.; Åkermark, B.; Sun, L. *Eur. J. Inorg. Chem.* **2005**, 2506−2513.
(27) Song, L.; Ge, J.; Zhang, X.; Liu, Y.; Hu, Q. *Eur. J. Inorg. Chem.* **2006**, 3204−3210.
(28) Hasan, M. M.; Hursthouse, M. B.; Kabir, S. E.; Abdul Malik, K. M. *Polyhydron* **2001**, *20*, 97−101.
(29) Lyon, E. J.; Georgakaki, I. P.; Reibenspies, J. H.; Darensbourg, M. Y. *Angew. Chem., Int. Ed.* **1999**, *38*, 3178−3180.
(30) Chen, L.; Wang, M.; Gloaguen, F.; Zhang, P.; Zhao, Z.; Sun, L. *Chem.—Eur. J.* **2012**, DOI: 10.1002/chem.201201326.
(31) Gloaguen, F.; Morvan, D.; Capon, J.-F.; Schollhammer, P.; Talarmin, J. *J. Electroanal. Chem.* **2007**, *603*, 15−20.
(32) Vannucci, A. K.; Wang, S.; Nichol, G. S.; Lichtenberger, D. L.; Evans, D. H.; Glass, R. S. *Dalton Trans.* **2010**, *39*, 3050−3056.
(33) Wright, R. J.; Zhang, W.; Yang, X.; Fasulo, M.; Tilley, T. D. *Dalton Trans.* **2012**, *41*, 73−82.
(34) Izutsu, K. *Acid-Base Dissociation Constants in Dipolar Aprotic Solvents*; Blackwell Scientific Publishers: Oxford, UK, 1990.
(35) Berning, D. E.; Noll, B. C.; DuBois, D. L. *J. Am. Chem. Soc.* **1999**, *121*, 11432−11447.
(36) Kilgore, U. J.; Roberts, J. A. S.; Pool, D. H.; Appel, A. M.; Stewart, M. P.; DuBois, M. R.; Dougherty, W. G.; Kassel, W. S.; Bullock, R. M.; DuBois, D. L. *J. Am. Chem. Soc.* **2011**, *133*, 5861−5872.
(37) King, R. B. *Organometallic Syntheses*; Academic Press: New York, 1965; Vol. *I*.
(38) Testaferri, L.; Tingoli, M.; Tiecco, M. *J. Org. Chem.* **1980**, *45*, 4376−4380.
(39) Jackstell, R.; Klein, H.; Beller, M.; Wiese, K.-D.; Röttger, D. *Eur. J. Org. Chem.* **2001**, 3871−3877.